



S.I. : 2022 CMBE Young Innovators

# Encapsulation of Manganese Porphyrin in Chondroitin Sulfate-A Microparticles for Long Term Reactive Oxygen Species Scavenging

FEI SAN LEE,<sup>1</sup> KAYLA E. NEY,<sup>1</sup> ALEXANDRIA N. RICHARDSON,<sup>1</sup> REBECCA E. OBERLEY-DEEGAN,<sup>2</sup> and REBECCA A. WACHS <sup>1</sup>

<sup>1</sup>Department of Biological Systems Engineering, University of Nebraska-Lincoln, 4240 Fair St, Lincoln, NE 68583-0900, USA; and <sup>2</sup>Department of Biochemistry and Molecular Biology, University of Nebraska Medical Center, Omaha, NE 68198, USA

(Received 4 March 2022; accepted 28 September 2022; published online 14 October 2022)

Associate Editor Michael R. King oversaw the review of this article.

## Abstract

**Introduction**—Oxidative stress due to excess reactive oxygen species (ROS) is related to many chronic illnesses including degenerative disc disease and osteoarthritis. MnTnBuOE-2-PyP<sup>5+</sup> (BuOE), a manganese porphyrin analog, is a synthetic superoxide dismutase mimetic that scavenges ROS and has established good treatment efficacy at preventing radiation-induced oxidative damage in healthy cells. BuOE has not been studied in degenerative disc disease applications and only few studies have loaded BuOE into drug delivery systems. The goal of this work is to engineer BuOE microparticles (MPs) as an injectable therapeutic for long-term ROS scavenging.

**Methods**—Methacrylated chondroitin sulfate-A MPs (vehicle) and BuOE MPs were synthesized *via* water-in-oil polymerization and the size, surface morphology, encapsulation efficiency and release profile were characterized. To assess long term ROS scavenging of BuOE MPs, superoxide scavenging activity was evaluated over an 84-day time course. *In vitro* cytocompatibility and cellular uptake were assessed on human intervertebral disc cells.

**Results**—BuOE MPs were successfully encapsulated in MACS-A MPs and exhibited a slow-release profile over 84 days. BuOE maintained high potency in superoxide scavenging after encapsulation and after 84 days of incubation at 37 °C as compared to naked BuOE. Vehicle and BuOE MPs (100 µg/mL) were non-cytotoxic on nucleus pulposus cells and MPs up to 23 µm were endocytosed.

**Conclusions**—BuOE MPs can be successfully fabricated and maintain potent superoxide scavenging capabilities up to 84-days. *In vitro* assessment reveals the vehicle and BuOE MPs are not cytotoxic and can be taken up by cells.

**Keywords**—Antioxidant, Oxidative stress, SOD mimic, Drug delivery, Degenerative disc disease.

## ABBREVIATIONS

BuOE	MnTnBUOE-2-PyP <sup>5+</sup>
ROS	Reactive oxygen species
SOD	Superoxide dismutase
CS-A	Chondroitin sulfate-A
MACS-A	Methacrylated chondroitin sulfate-A
MP	Microparticle
NP	Nucleus pulposus

## INTRODUCTION

Oxidative stress due to excess reactive oxygen species (ROS) contribute to the pathogenesis and progression of chronic illnesses. The accumulation of cellular damage caused by ROS over a person's lifespan are key drivers of the mechanisms in age-related diseases<sup>83</sup> such as degeneration of intervertebral discs<sup>61</sup> and articular cartilage,<sup>33</sup> which are highly linked to conditions such as chronic low back pain<sup>22,87</sup> and osteoarthritis,<sup>10,11</sup> respectively. Globally, up to 23% of the population suffer from low back pain<sup>35</sup> and 3.8% suffer from knee osteoarthritis<sup>21</sup> and these diseases are the leading causes of pain and disability worldwide.<sup>21,78</sup> Hence, there is a need for long-lasting treatments that can effectively treat degenerative joint diseases to alleviate orthopedic pain. Instead of targeting the etiological factors such as ROS, most clinical treatments focus on managing pain with physical therapy, opioid prescriptions, and non-steroidal anti-inflammatory drugs (NSAIDs). Unfortunately, NSAIDs can have complications<sup>9,49,64,72,82</sup> and only have short-term efficacy; therefore, requiring repeated doses. For orthopedic diseases that do not respond to

Address correspondence to Rebecca A. Wachs, Department of Biological Systems Engineering, University of Nebraska-Lincoln, 4240 Fair St, Lincoln, NE 68583-0900, USA. Electronic mail: rebecca.wachs@unl.edu

pain-relief medications, invasive surgery to treat the painful degenerated disc (lumbar discectomy) or knee (knee arthroplasty) is performed, which is expensive and can have adverse effects.<sup>12,32,79</sup> Thus, minimally invasive treatments that target the underlying biological mechanisms of the disease, such as oxidative stress and ROS, are needed.

ROS are defined as molecules containing oxygen and one or more unpaired electrons. Primarily, ROS are byproducts of mitochondrial respiration and include superoxide ( $O_2^{\cdot-}$ ), hydroxyl ( $OH^{\cdot}$ ) and hydrogen peroxide ( $H_2O_2$ ). These reactive molecules are capable of damaging lipid membranes, proteins and DNA but also serve as a crucial signaling molecule for cellular metabolism, differentiation, and proliferation.<sup>58</sup> Under normal conditions, endogenous antioxidant enzymes such as superoxide dismutase (SOD) and catalase convert ROS into less harmful species to regulate a healthy oxidative balance and protect cells from oxidative damage.<sup>39</sup> However, in diseased states, decreased antioxidant levels and overproduction of ROS surpass the capacity of the natural defense mechanisms, resulting in oxidative stress.<sup>8</sup> Excess ROS cause oxidative damage by oxidizing proteins, lipids, and DNA beyond the cell repair mechanism and activating apoptotic signaling pathways which can lead to cell death.<sup>57,67</sup> Further, high levels of ROS trigger local cells to produce pro-inflammatory cytokines such as tumor necrosis factor-alpha (TNF- $\alpha$ )<sup>17</sup> and interleukin-1-beta (IL-1 $\beta$ )<sup>59</sup> which causes mitochondrial damage and consequently, more ROS production<sup>46</sup> and aggravation of the disease pathology.<sup>26,61</sup> In knee osteoarthritis, activation of ROS-sensitive transcription factors such as nuclear factor kappa-B (NF- $\kappa$ B), activator protein-1 (AP-1), specificity protein (SP)-1 and hypoxia inducible factor (HIF)-1a can lead to cartilage remodeling and synovium inflammation.<sup>33</sup> Oxidative stress in the intervertebral disc activates pathways such as the NF- $\kappa$ B and mitogen-activated protein kinase (MAPK) pathway, which can lead to inflammation and matrix degradation.<sup>30</sup> Based on evidence that ROS plays a crucial role in oxidative damage, inflammation and disease progression, antioxidant therapy that scavenges excess ROS has gained attention for the treatment of oxidative stress-related diseases, such as knee osteoarthritis and degenerative disc disease.

Native antioxidant enzymes such as SOD are not ideal therapeutic agents due to their poor stability, inability to cross cell membranes, and short half-life *in vivo*.<sup>38,60</sup> Thus, researchers have developed synthetic antioxidants that imitate the activity and characteristics of endogenous antioxidant enzymes to address these drawbacks. One example is manganese porphyrin, a synthetic SOD mimic that actively scavenges

$O_2^{\cdot-}$ .<sup>5,25</sup> and exhibits self-renewal properties due to the ability of the manganese core to both donate and accept electrons.<sup>5</sup> A specific type of manganese porphyrin, MnTnBuOE-2-PyP<sup>5+</sup> (BuOE) potently scavenges  $O_2^{\cdot-}$  while also activating nuclear factor erythroid 2-related factor (Nrf2), a transcription factor that upregulates production of endogenous antioxidants<sup>86</sup> to help further reduce ROS and restore oxidative balance.<sup>38</sup> BuOE is also able to regulate cellular inflammation by blocking NF- $\kappa$ B activation in chondrocytes, thereby inhibiting proinflammatory cytokine production and reducing inflammation.<sup>19</sup> *In vivo*, topical application of BuOE is also effective at reducing inflammation and prevented itching in an allergic dermatitis mouse model,<sup>7</sup> and is currently being investigated to treat cancer<sup>75</sup> and aortic valve sclerosis.<sup>2</sup> BuOE has cleared a myriad of toxicology and safety testing<sup>28,65</sup> and is currently undergoing Phase I and II clinical trials as a protector for healthy tissues against radiation-induced oxidative damage during cancer radiation therapy (ClinicalTrials.gov ID NCT02655601, NCT03608020, NCT03386500).<sup>18,48,55</sup> The non-toxic and anti-inflammatory properties of BuOE combined with its strong antioxidant capacity make it an ideal therapeutic for oxidative-stress related diseases which exhibit chronic inflammation. No previous works have investigated the potential of BuOE as a therapeutic for degenerative disc disease.

Despite great promise of using BuOE as an antioxidant and anti-inflammatory drug, adverse effects such as decreased blood pressure were observed after systemic injection into rodents<sup>69,70</sup> and dogs.<sup>28</sup> In addition, systemically delivered drugs may not reach targeted tissues with limited blood supply, such as the intervertebral disc.<sup>24</sup> To overcome these side effects, microparticle drug delivery systems with tunable biomaterial degradation and release kinetics have been developed.<sup>27,51</sup> Microparticles (MPs) directly injected into local tissue typically retain at the site of administration<sup>42,47,66</sup> and have longer residence time compared to solution or free suspension delivery<sup>13</sup>; thus, reducing the need for repeated dosing. Further, MPs can be exploited for intracellular or extracellular targeting due to their size range between 1 and 100  $\mu$ m. Polymeric MPs have been developed for other synthetic antioxidants,<sup>56</sup> but no previous studies have reported microparticle systems for manganese porphyrins. Therefore, the overarching goal of this research is to develop BuOE MPs as potential long-term therapeutic to relieve oxidative stress in degenerative disc disease and osteoarthritis.

In this work, we have successfully loaded BuOE into methacrylated chondroitin sulfate-A (MACS-A) microparticles for proposed long-term ROS scavenging. We characterized encapsulation efficiency, release

profiles and long-term superoxide scavenging activity of BuOE MPs and conducted *in vitro* experiments to assess cytocompatibility and cellular uptake.

## METHODS

### *Fabrication of BuOE MPs*

#### *Chondroitin Sulfate-A Methacrylation*

BuOE is highly cationic in nature and because of this property it can easily be loaded into anionic chondroitin sulfate-A (CS-A) MPs *via* electrostatic interactions. CS-A are glycosaminoglycans and a native component of extracellular matrix in cartilaginous tissues, such as knee cartilage<sup>63</sup> and intervertebral discs.<sup>73</sup> CS-A MPs have been previously used for growth factor delivery,<sup>29</sup> and as a natural biomaterial for drug delivery and tissue engineering scaffolds.<sup>84</sup> We adapted techniques from Lim *et al*<sup>54</sup> to fabricate cross-linkable methacrylated chondroitin sulfate-A (MACS-A) MPs for BuOE delivery. Chondroitin sulfate was chemically-modified through a methacrylation process<sup>62,68,74</sup> to synthesize cross-linkable monomers for microparticle formation. Briefly, 125 mg/mL Chondroitin sulfate-A (CS-A) (Sigma-Aldrich, C9819) was dissolved in ultrapure water overnight at room temperature. 10 mL of methacrylic anhydride (Sigma-Aldrich, 276685) was added in 1 mL increments into the dissolved chondroitin sulfate-A solution on ice while maintaining pH 8–10 with 5 M sodium hydroxide. The solution was stirred at 4 °C for 16 h then precipitated in acetone (Fisher Scientific, A18-20) at a 1:20 MACS-A:acetone volume ratio. The methacrylated CS-A (MACS-A) precipitate was filtered through a Q5 medium porosity filter paper (Fisher Scientific, 09-790-2G) in a Buchner funnel, (VWR, 89038-128) and reconstituted in ultrapure water for approximately 24 h. Once fully dissolved, MACS-A was purified through a 10,000 dalton molecular weight cutoff (MWCO) dialysis cassette (ThermoFisher, 87733) against ultrapure water for 72 h at room temperature with dialysate changes every 12 h to remove any unreacted MACS-A. After dialysis, the final MACS-A product was obtained after 72 h of lyophilization (FreeZone benchtop freeze dryer, Labconco). Proton nuclear magnetic resonance (<sup>1</sup>H-NMR) spectroscopy using a Bruker Avance 600 MHz spectrometer was used to determine successful CS-A methacrylation. To prepare samples for NMR, lyophilized MACS-A (10 mg/mL) was dissolved in deuterium oxide (Sigma, 1133660100) overnight. <sup>1</sup>H-NMR spectrum was analyzed using TopSpin 3.6.1 software (Bruker). Degree of methacrylation was calculated by comparing the integral area under peak CS-related proton peaks ~ 1.84

ppm to methyl methacrylate peak ~ 1.91 ppm.<sup>81</sup> MACS-A with methacrylation percentages ranging from 112.1 to 134.5 were used to fabricate MPs in this study (Supplemental Fig. 1).

### *Vehicle and BuOE MP Fabrication*

Figure 1 shows an overview of the MP fabrication process and an illustration of a MACS-A MP with encapsulated BuOE. MACS-A MPs were formed by single water-in-oil emulsion and free radical polymerization. BuOE was provided by Dr. Rebecca Oberley-Deegan from University of Nebraska-Medical Center. First, 126.4 mg/mL MACS-A was fully reconstituted overnight at 4 °C in 1X phosphate buffered saline (1X PBS) with dissolved 3.0 mg BuOE. Vehicle MPs are unloaded MPs and were fabricated with MACS-A dissolved in pure 1X PBS without BuOE. Ammonium persulfate (0.3 M, Sigma, A3678) and tetramethylethylenediamine (0.3 M, Sigma, T7024) were freshly prepared in ultrapure water then mixed into the MACS-A solution at 0.0682:1 volume ratio to MACS-A. To create a water-in-oil emulsion, this aqueous mixture was pipetted dropwise into cold 100% corn oil in a conical flask and dispersed through homogenization at 2000 rpm (T25 Digital S001 LR, IKA) with a 18G dispersing tool (IKA, 593400) for five minutes. The flask was subsequently sealed, and the emulsion was bubbled under nitrogen gas to remove atmospheric oxygen which can react with free radicals and prevent cross-linking. Under this inert environment, MACS-A polymerization was initiated by heating the emulsion in a 50 ± 5 °C water bath. Polymerization continued for 35 min with a constant agitation rate of 50 rpm on a magnetic stir plate. The cross-linked MPs were retrieved by separating the corn oil through centrifugation at 3000 rpm (Sorvall ST40 Centrifuge and TX-1000 Swing Bucket Rotor). MPs were washed three times with ultrapure water and repeated centrifugation to remove residual corn oil. After washes, aliquots of MP solution were removed for size and BuOE encapsulation efficiency analysis. The remaining MP solution was lyophilized for 72 h and stored at – 20 °C.

### *Vehicle and BuOE MP Characterization*

#### *BuOE Encapsulation and Polymerization Efficiency*

An absorbance assay was used to estimate the encapsulation efficiency of BuOE. Aliquots of BuOE MPs removed after MP fabrication were pipette into a clear bottomed black 96 well plate in triplicate and the absorbance was measured at 455 nm using an area scan mode in a microplate reader and Gen5 software (Synergy H1, BioTek). BuOE solutions at known concentrations (100–1000 µg/mL) were prepared and



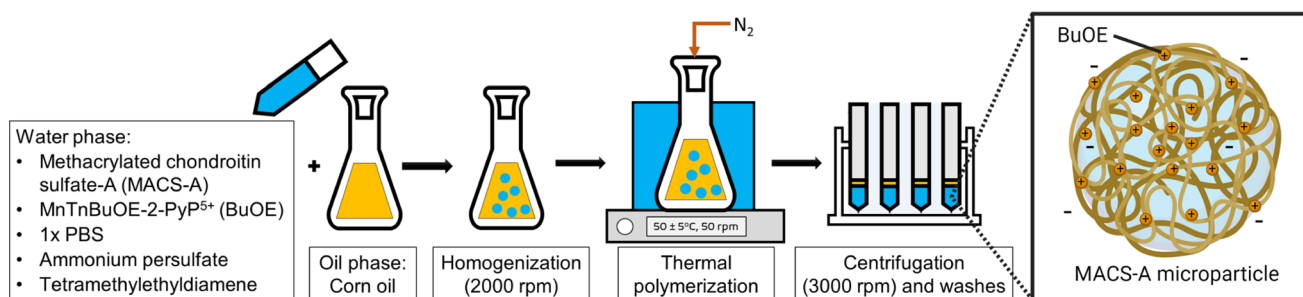


**FIGURE 1.** MACS-A microparticle fabrication with BuOE encapsulation *via* water-in-oil emulsion thermal polymerization. MACS-A as the cross-linking monomers constitutes the water phase solution. When fabricating BuOE microparticles, dissolved BuOE is mixed in the water phase solution with MACS-A. The oil and water phase solutions were homogenized to create an emulsion. Under nitrogen purged condition, thermal polymerization initiates MACS-A cross-linking. MPs were retrieved *via* centrifugation and washed then lyophilized to form the final product.

absorbance was measured at 455 nm using a microplate reader. The absorbance was plotted as a function of BuOE concentration to generate a standard curve and linear regression for calculating the amount of BuOE encapsulated in the MPs. Vehicle MPs were included as blanks. Based on the standard curve, the calculated BuOE concentration in mg/mL of the BuOE MPs were multiplied to the final volume of MP solution to obtain the total weight of encapsulated BuOE. To obtain the encapsulation efficiency, the weight of BuOE was divided over the weight of BuOE added during fabrication then multiplied by 100%. To determine MACS-A polymerization efficiency, lyophilized MPs were weighed and divided by the initial MACS-A weight then multiplied by 100%.

#### Vehicle and BuOE MP Size Quantification

To quantify MP size, vehicle MPs and BuOE MPs were stained with 1, 9-dimethylmethylene blue (DMMB, Biocolor, B1005) to provide good contrast for imaging. DMMB is a dye that stains the sulfated polysaccharide component of sulfated glycosaminoglycan chains. MPs were incubated for 1 h with DMMB dye on a shaker plate (120 rpm) at room temperature. Brightfield images were taken at 10X and 40X (four images per magnification) using an inverted widefield DMI3000B microscope (LEICA). Images of MPs were analyzed using ZEN 3.0 Lite Intellesis (Carl Zeiss Microimaging, Inc) to quantify the size distribution of the MPs. At least 600 DMMB-stained MPs were quantified per batch from  $n = 3$  vehicle MP batches and  $n = 3$  BuOE MP batches.

#### Vehicle and BuOE MP Surface Morphology

Scanning electron microscopy (SEM) was used to observe surface morphology of the fabricated MPs. To prepare MPs for SEM, lyophilized vehicle and BuOE MPs were fixed in 4% paraformaldehyde (PFA) (Sigma Aldrich, 441244) for 10 min then triple-washed in

1X PBS for 15 min on a tube rotator at 10 rpm. The fixed MPs were dehydrated through a series of graded ethanol (30%, 50%, 70%, 85%, 90%, 95%, 100%) and ethanol-hexamethyldisilazane (Electron Microscopy Services, 16700) (25%, 50%, 75%, 100% HMDS) solutions. Final MP resuspension in 100% HMDS were transferred onto a round glass coverslip and left to fully evaporate overnight in the fume hood. The coverslips with dehydrated MPs were mounted on pin stubs (Ted Pella, 16111) with conductive tape and sputter coated with Au (Cressington 106 Auto Sputter Coater) for 20 s. MPs were imaged on a FEI Helios SEM 660 at 20 kV, 0.4 nA at 5,000X, 10,000X, 250,000X.

#### BuOE MP Superoxide Scavenging and Appearance Over Time

To test the superoxide scavenging ability and long-term stability of BuOE MPs at physiologically relevant conditions, three batches of BuOE MPs (80  $\mu\text{g/mL}$  MP) and naked BuOE (0.4  $\mu\text{M}$ , 1254.53 g/mol) were resuspended in 10 mL 1X PBS (pH 7.3–7.5). BuOE MPs solutions were stored in a 37 °C oven for 84 days and 100  $\mu\text{L}$  aliquots were sampled before (day 0) and after 28, 56, and 84 days of incubation. The BuOE MP aliquots were centrifuged at 10,000 rpm for five minutes to separate the BuOE MPs (pellet) and released BuOE (supernatant) and stored at  $-20$  °C until all sampling points were completed. To measure stability of superoxide scavenging activity of the BuOE MP pellet and released BuOE in supernatant solutions, SOD Activity Kit (K335-100, BioVision) was used. In this assay, WST-1 is converted to WST-formazan (455 nm absorbance) when reduced by superoxide. WST-1 was added to all samples and allowed to equilibrate for 30 min at 4 °C prior to conducting the assay. To generate superoxide, xanthine oxidase (XO) provided by the kit was used. Absorbance of samples were read using a microplate reader pre- and 20 min



post-incubation with XO at 37 °C, 5% CO<sub>2</sub>. Equation 1 was used to calculate the percentage of superoxide scavenged. Briefly, the difference in absorbance in the sample before and after XO was compared to the difference of absorbance between Blank 1: “positive” controls without XO (no superoxide generated i.e. 100% superoxide scavenged) and Blank 3: XO only, negative controls without BuOE/antioxidants (maximum superoxide produced i.e. 0% superoxide scavenged).

$$\text{Superoxide scavenged(\%)} = \frac{(\text{AbsBlank 1} - \text{AbsBlank3}) - (\text{AbsSample before XO} - \text{AbsSample after XO})}{(\text{AbsBlank1} - \text{AbsBlank3})} \quad (1)$$

Brightfield images of BuOE MPs were taken on an inverted light microscope (Vistavision) at 10X on each sampling day to monitor any size or color changes.

#### BuOE Release Measurements

Supernatants of BuOE MPs were collected on days 0, 28, 56, 84 during the previous analysis and were used to determine release. Inductively couple plasma mass spectrometry (ICP-MS) was used to detect the amounts of BuOE in the supernatant solutions for each time-point. ICP-MS was used to quantify the release of BuOE from the vehicle MP over 84 days. To prepare samples for ICP-MS, samples were diluted 1:10 in 2% nitric acid containing 50 parts per billion gallium. Samples were then transferred into 96 well plates using an autosampler (Elemental Scientific, Inc (Omaha, NE) model SC-DX4). Each sample was run in aliquots of 100  $\mu\text{L}$  in triplicate with a 2% nitric acid rinse between each triplicate set. The ICP-MS (Agilent 7500cx, Santa Clara, CA) was run at a sample flow rate of 55–60  $\mu\text{L}/\text{min}$ . ICP-MS was conducted in mix reaction/collision mode with 3.5 mL/min hydrogen gas and 1.5 mL/min helium to remove interferences. The instrument was set to operate at forward power (1500 W) with a carrier argon flow of 1.0 L/min and make-up flow of 0.1 L/min. The spray chamber used a micronebulizer (Glass Expansion) maintained at 2 °C. Samples containing supernatant were compared to a standard dilution of BuOE with a concentration range of 1.3 nM to 0.399  $\mu\text{M}$  naked BuOE prepared and processed in the same manner as the supernatant samples. Parts per billion measurements from the unknown samples were compared to the measurements from the standard to determine the unknown concentrations.

#### BuOE Microparticle Cytocompatibility and Cellular Interaction

##### Vehicle and BuOE MP Disinfection and Media Preparation

Prior to *in vitro* testing, MPs were disinfected with an ethanol soak. Lyophilized vehicle MPs (3 distinct batches) and BuOE MPs (3 distinct batches) were resuspended in 1X PBS in 100% ethanol at 2 mg/mL and placed on a tube rotator at 10 rpm for 1 h. Then,

MPs were isolated through centrifugation at 10,000 rpm for five minutes and washed once with 1X PBS. After washing, the disinfected MPs were resuspended in complete nucleus pulposus (NP) culture media, which consists of basal NP cell medium supplemented with 1% Penicillin–Streptomycin, 1% growth supplement and 2% fetal bovine serum (ScienCell, 4801) to achieve 100  $\mu\text{g}/\text{mL}$  MPs for *in vitro* experiments.

##### Nucleus Pulposus Cell Culture

Nucleus pulposus (NP) cells are the matrix-producing cells in the core of intervertebral discs. Previous research have elucidated ROS as an instigator for cellular senescence and catabolic phenotype in human NP cells.<sup>23</sup> Due to these findings, *in vitro* testing of BuOE MPs was performed on human NP cells. Human NP cells (ScienCell, 4800) from three separate donors were expanded on poly-L-Lysine (PLL)-coated (2  $\mu\text{g}/\text{cm}^2$ , Sciencell, 0413) T-75 flasks and used at passages 3–4. For cell viability and metabolic activity studies, NP cells were seeded on PLL-coated 48-well plates at recommended seeding density of 5,000 cells/ $\text{cm}^2$ . For MP uptake studies, NP cells were seeded on Permanox® 8-well chamber slides (177445PK, Thermo Scientific) at 5,000 cells/ $\text{cm}^2$ . In all well types, cells were allowed to adhere for 24 h, then the media was replaced with either complete NP media (control), vehicle MPs in media (100  $\mu\text{g}/\text{mL}$ ) or BuOE MPs in media (100  $\mu\text{g}/\text{mL}$ ) and cells were cultured for three days for viability and metabolic activity assessments or four days for MP uptake experiment. During viability and metabolic activity analysis, MP-media solution would need to be removed during assays; therefore,

three separate sets of well plates with NP cells were prepared with one for each of the three assay time-points (days 1, 2, 3 post-MP treatment). Throughout the experiments, NP cells were cultured under hypoxic conditions (5% CO<sub>2</sub>, 3.5% O<sub>2</sub>, 91.5% N<sub>2</sub>) in a hypoxia incubator chamber (Stem Cell Technologies, 27310) in a 37 °C incubator. Cell health and proliferation was monitored using brightfield imaging on an inverted plate imager (Cytation 1, Imaging Reader, BioTek) at 4X magnification on days 1, 2, and 3.

#### *Vehicle and BuOE MP Cytocompatibility*

Vehicle MP and BuOE MP cytocompatibility was assessed using a cytotoxicity assay and a metabolic activity assay. A CYQUANT™ LDH cytotoxicity assay (C20300, ThermoScientific) was used to measure cell death. NP cells were cultured in six replicate wells in 48-well plates and treated with or without vehicle and BuOE MPs, as stated above. To perform LDH cytotoxicity assay, three wells were lysed with Lysis buffer (from kit) for 45 min to obtain maximum LDH controls per experimental group. After 45-min incubation, duplicates of 50 μL media aliquots from the lysed cells (max LDH), controls, vehicle MPs, BuOE MPs and respective MP media blanks were transferred to a 96-well plate and assay was performed according to manufacturer's instructions. Percent cytotoxicity was calculated based on Eq. 2.

$$\% \text{Cytotoxicity} = \frac{(\text{Controls or MP treated LDH activity})}{(\text{Maximum LDH activity})} * 100\% \quad (2)$$

After removing media aliquots for LDH assay, cellular metabolic activity was assessed using AlamarBlue HS cell viability reagent (A50100, ThermoFisher). Cells were incubated with 10% v/v AlamarBlue reagent in media for 2 h at 37 °C under hypoxia. Absorbance of the media was read at 570 nm and 600 nm and the cellular metabolic activity was calculated based on the percent of AlamarBlue reduction as described in the manufacturer's protocol. LDH and AlamarBlue experiments were repeated to test cytocompatibility three batches of each vehicle MPs and BuOE MPs on three separate NP cell donors.

#### *Cellular Uptake of Vehicle and BuOE MPs*

To assess whether vehicle MPs and BuOE MPs can be internalized in NP cells, immunocytochemistry and confocal microscopy was performed to closely visualize NP cells and MPs after incubation period. NP cells were cultured on 8-well chamber slides as stated above then fixed with 4% paraformaldehyde (PFA) for 15 min and triple-washed three times with 1X PBS for

10 min. Cells were permeabilized with blocking buffer solution consisting of 0.3% v/v TritonX-100 (93443, Sigma-Aldrich) and 3% v/v goat serum (G9023, Sigma-Aldrich) in 1X PBS for 10 min. Vehicle MPs and BuOE MPs were labelled with primary antibody mouse anti-CS56 (1:200, C8035, Sigma-Aldrich) in blocking buffer at 4 °C overnight and secondary antibody anti-mouse AlexFluor647 (1:1000, Ab150118, Abcam) for one hour at room temperature. Cells were also stained with a cytoskeletal marker using Phalloidin-iFluor488 reagent (1:1000, ab175753, Abcam) during secondary antibody incubation. ProLong Gold antifade reagent (P36934, Invitrogen) and a no.1.5 glass coverslip was applied on the stained cells. Fluorescent images were taken using an upright ZEISS LSM 510 confocal microscope (Carl Zeiss Microimaging, Inc.). Ten images of internalized MPs in cells were taken at 40X magnification and the MP diameter was measured in 24 to 35 MPs using Zen Blue 3.2 software (Carl Zeiss Microimaging, Inc.).

#### *Statistics*

All analyses were carried out using Prism version 7.03 (GraphPad). MACS-A polymerization efficiency were compared using unpaired t-test. MP size distribution did pass a Shapiro–Wilk normality test, so Mann–Whitney test was used to compare MP size. A minimum of three batches of vehicle MPs and BuOE MPs were used. A histogram of MP diameter with 2.5 μm bin size was generated and a multiple t-test was conducted to compare the percent frequency per bin. Long term BuOE activity, cytotoxicity and cell metabolic activity were normalized to controls and significance was analyzed *via* a two-way ANOVA with a Tukey's post-hoc test with a significance of 0.05. For MP uptake assessment, average diameter of internalized vehicle MPs and BuOE MPs were compared using unpaired t-test.

## RESULTS

### *BuOE was Successfully Encapsulated in MACS-A MPs*

MACS-A MPs were successfully fabricated and implemented as a drug delivery vehicle for BuOE. Vehicle MPs were confirmed to be cross-linked MACS-A as seen in the round purple bodies stained with DMMB which stains chondroitin sulfate (Fig. 2a). BuOE is water-soluble and forms a dark brown solution. When mixed with MACS-A solution, BuOE was successfully encapsulated in MACS-A MPs after cross-linking, as seen in images of brown-colored BuOE MPs with and without DMMB staining

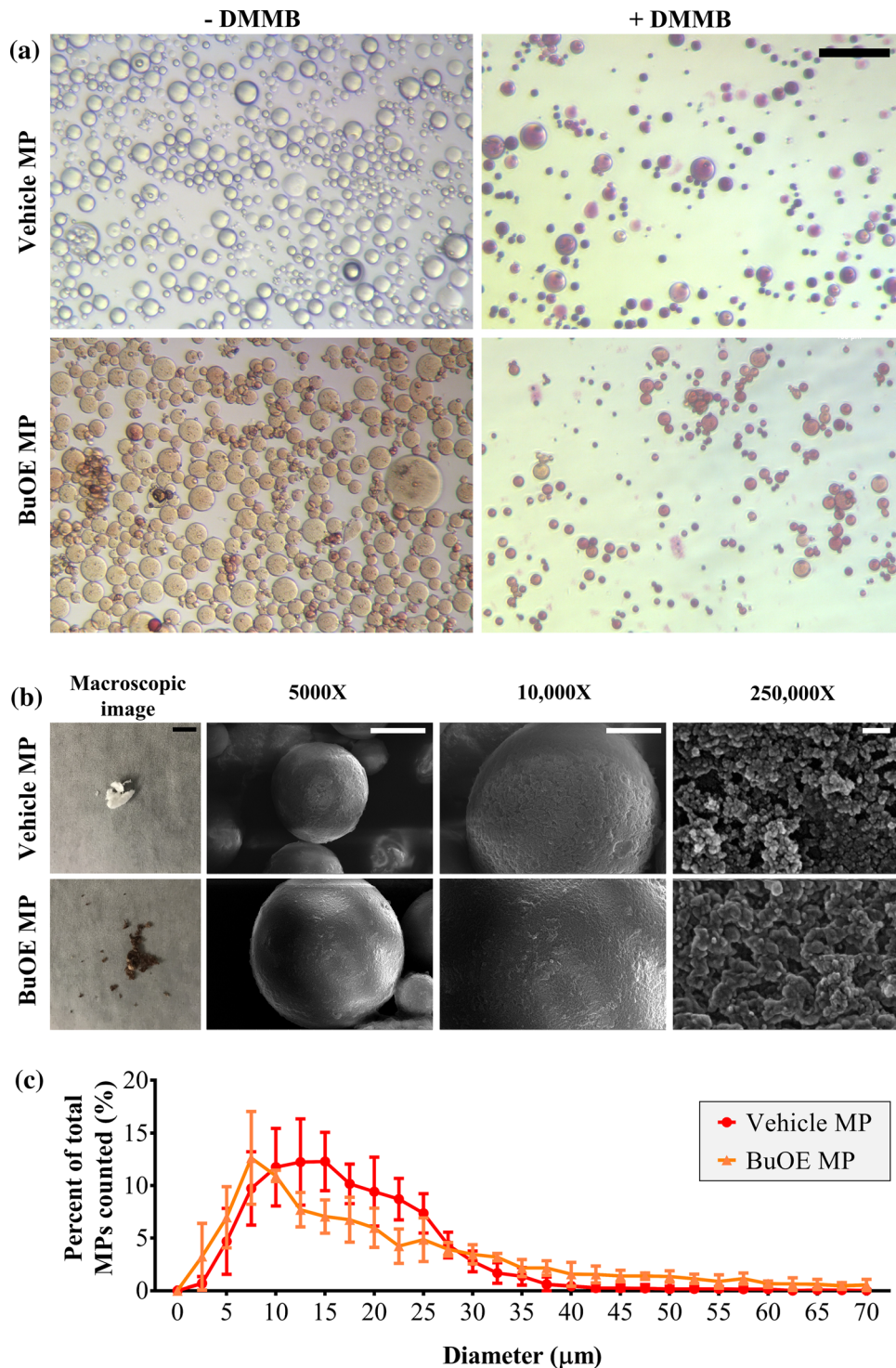


**FIGURE 2.** BuOE were successfully encapsulated into MACS-A microparticles. (a) Color images show successful fabrication of vehicle MACS-A microparticles (MPs) and encapsulated BuOE MACS-A MPs. DMMB staining (purple) in vehicle MACS-A MPs confirm presence of chondroitin sulfate which was also visible in BuOE MPs. Scale bar: 100  $\mu\text{m}$ . (b) Photo of final lyophilized MPs: vehicle MPs, BuOE MPs. BuOE MPs stayed encapsulated in powder form even after lyophilization as seen by the dark brown color compared to vehicle MPs. SEM images showed no difference in surface microstructure of vehicle and BuOE MPs at 5,000x, 10,000  $\times$  and 250,000x. Scale bars from left to right: 50 mm, 10  $\mu\text{m}$ , 5  $\mu\text{m}$ , 100 nm. (c) Percent frequency distribution of MP diameter were not significantly different between vehicle and BuOE MPs and within  $n = 3$  batches per group. Average diameter of vehicle and BuOE MPs were  $17.44 \pm 7.48 \mu\text{m}$  and  $22.02 \pm 15.26 \mu\text{m}$  (Mean  $\pm$  SD,  $n = 3$  batches), respectively.



**TABLE 1.** Summarizes the characterized properties of vehicle MPs and BuOE MPs.

	Vehicle MP(Mean $\pm$ SD, $n = 3$ )	BuOE MP(Mean $\pm$ SD, $n = 3$ )
Diameter, average $\pm$ SD ( $\mu\text{m}$ )	17.44 $\pm$ 7.48	22.02 $\pm$ 15.26 <sup>#</sup>
MACS-A polymerization efficiency (%)	49.9 $\pm$ 8.0	29.0 $\pm$ 6.0 *
BuOE encapsulation efficiency (%)	–	3.1 $\pm$ 0.5
BuOE:MACS-A weight ratio ( $\mu\text{g}/\text{mg}$ )	–	6.3 $\pm$ 0.4

<sup>#</sup> $p < 0.0001$  comparing BuOE MP to vehicle MP.

\* $p < 0.05$  comparing BuOE MP to vehicle MP.

(Fig. 2a). Vehicle and BuOE MP diameters ranged between 1 and 121  $\mu\text{m}$ . The average MP diameter for BuOE MPs were significantly higher than vehicle MPs (Table 1), although not substantially (22.02  $\pm$  15.26  $\mu\text{m}$  v. 17.44  $\pm$  7.48  $\mu\text{m}$ ). Figure 2c plots the frequency distribution of MP diameter and analysis revealed no significant differences in the percentage of MPs per diameter suggesting vehicle and BuOE MPs have similar size distribution. After lyophilization, vehicle MPs form a white powder (Fig. 2b) and BuOE MPs form a dark brown powder (Fig. 2b). This suggests that BuOE remains encapsulated inside or bound onto the MPs and is not affected by lyophilization. Encapsulation efficiency of BuOE was 3.1% (Table 1). The encapsulated BuOE MP weighs approximately 6.3  $\mu\text{g}$  BuOE per mg of MACS-A (Table 1). Another property that was characterized is MACS-A polymerization efficiency determined by weight. MACS-A polymerization efficiency was significantly decreased in BuOE MPs compared to vehicle MPs (Table 1). This suggests that BuOE encapsulation could be interfering with MACS-A cross-linking; therefore, resulting in a lower yield of MACS-A in the BuOE MPs. Reduced MACS-A cross-linking could also explain the low encapsulation efficiency for BuOE MPs. Despite this, SEM revealed vehicle and BuOE MPs are spherical in shape and have similar rough surface microstructure (Fig. 2b). Further, at 250,000X the nanostructure of vehicle MPs and BuOE MPs are similar and exhibit a dense porous network. Overall, this data concludes that MACS-A MPs can be successfully used as a delivery vehicle for BuOE.

#### *Encapsulated and Released BuOE Maintained Superoxide Scavenging Ability*

Naked BuOE and BuOE MPs were stored at 37 °C in 1X PBS (pH 7.3–7.5) to study the effects of temperature on the MP morphology, drug release, and stability of superoxide scavenging activity. Throughout the 84-day incubation, BuOE MPs did not change in shape or size, however, the color of BuOE MPs on day 84 were less brown compared to day 0 (Fig. 3a). This led to further investigation to quantify the release of BuOE from MPs.

Results from ICP-MS analysis revealed that BuOE was released from the MPs into the supernatant over time (Fig. 3b). Average BuOE released from three MP batches significantly increased from 7.56  $\mu\text{g}$  on day 0 to 13.4, 16.3, 18.5  $\mu\text{g}$  on days 28, 56 and 84, respectively. Statistical analysis did not detect significant differences in released BuOE between the three distinct MP batches.

To assess if encapsulated and released BuOE was still able to scavenge superoxide, a superoxide scavenging assay was performed. BuOE MP pellet and supernatant each scavenged around 80% of superoxide present and was not significantly different from naked BuOE on day 0 (Fig. 3c). This data suggests that BuOE encapsulation does not inhibit its function to scavenge superoxide and at 0.4  $\mu\text{M}$  BuOE, BuOE MPs provides high enough potency to scavenge superoxide in long term superoxide scavenging study. Over time, BuOE MP pellet and released BuOE (supernatant) had no significant differences in superoxide scavenging activity; however, naked BuOE drastically decreased in scavenging activity from day 0 to day 28 and decreased further on days 56 and 84. BuOE MP pellet and supernatant maintained significantly higher superoxide scavenging activity compared to naked BuOE on days 28, 56 and 84, scavenging between 46.9–80.2% and 73.0–85.9% of superoxide, respectively. These findings indicate that BuOE MPs have the potential ability to release drug at a treatment site and scavenge superoxide for months at physiological temperature and pH.

#### *BuOE MPs are Cytocompatible with Human NP Cells In Vitro*

NP cell proliferation was not hindered by the presence of 100  $\mu\text{g}/\text{mL}$  vehicle and BuOE MPs and cells reached confluency similar to control group by day 3 post-treatment (Fig. 4a). Cell death and metabolic activity assays demonstrate that vehicle and BuOE MPs are cytocompatible with human NP cells *in vitro* (3 donors). Cell death measured by the LDH assay indicated low, less than 10%, cytotoxicity in controls, vehicle MPs, and BuOE MPs at all time points (Fig. 4b). Percent cytotoxicity of vehicle MPs did not significantly differ from controls. Interestingly, BuOE MPs had sig-

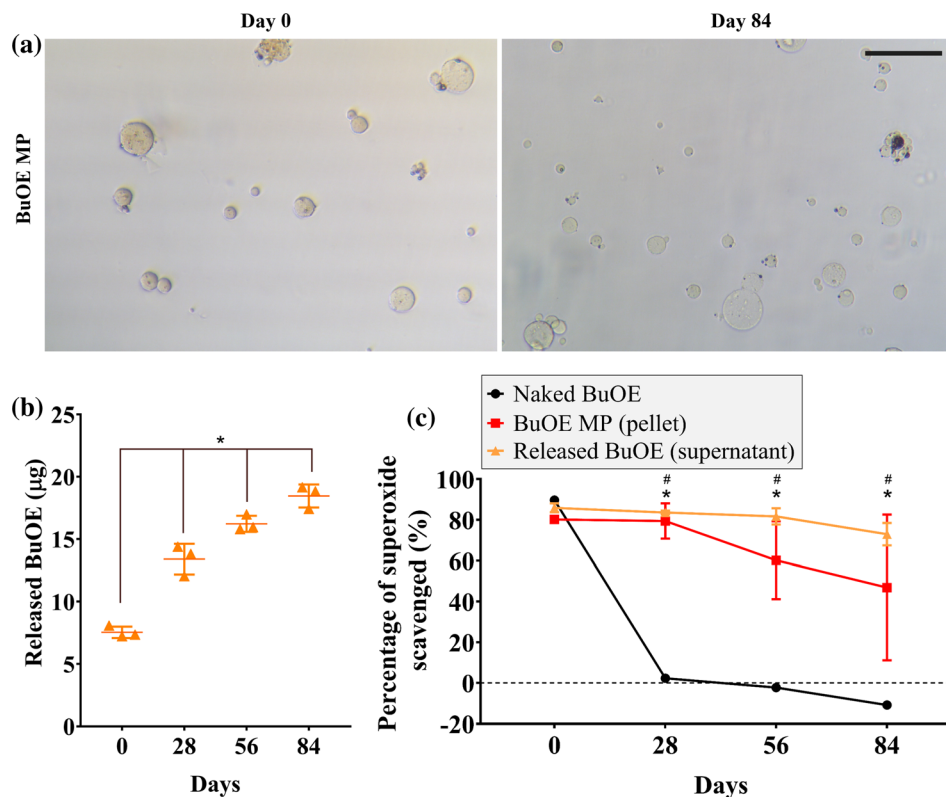


**FIGURE 3.** Encapsulated and released BuOE maintained scavenging activity in vitro. (a) Images of BuOE MPs over time before and 84 days after 37 °C incubation. BuOE MPs became more clear (less brown) compared to day 0 (before incubation) which may indicate release of BuOE without degradation of vehicle MPs. Scale bar: 100  $\mu\text{m}$ . (b) ICP-MS detected manganese in supernatant of BuOE MP samples after incubation suggesting release of BuOE out from MPs after over 84 days. (c) Before 37 °C incubation (day 0), average superoxide scavenging activity of naked BuOE (0.4  $\mu\text{M}$ ) was not significantly different compared to BuOE MPs (pellet and supernatant). After 28, 56 and 84 days of incubation, scavenging activity of naked BuOE significantly decreased from 89.7% to 2.3%, -2.3 and -10.9%, respectively. BuOE MP pellet and supernatant did not significantly differ over time. Released BuOE in supernatant scavenged significantly higher amounts of superoxide (83.6, 81.7, 73.0%) after 28, 56 and 84 days of incubation while BuOE MP pellets scavenged 79.4, 60.2, 46.9% of superoxide. Error bars represent the average from  $n = 3$  MP batches. \* $p < 0.05$ .

nificantly lower levels of LDH compared to vehicle MPs on days 1 and 3 and controls on day 1 post-treatment, which might be due to BuOE's antioxidative property and ability to maintain cell health. In addition, metabolic activity of both vehicle MP-treated and BuOE MP-treated cells normalized to same-day controls did not significantly change on days 1, 2 and 3 post treatment (Fig. 4c). This suggests vehicle MPs and BuOE MPs did not impact cellular metabolism. No significant differences in cytotoxicity and cell metabolic activity were detected between MP batches or NP cell donors (Supplementary Fig. 2) indicating there were no donor or batch-to-batch variability for MP cytocompatibility. These results demonstrate that vehicle MPs and BuOE MPs are non-cytotoxic to human NP cells.

#### NP Cells Uptake Vehicle and BuOE MPs

NP cells readily take up both vehicle MPs and BuOE MPs (Fig. 5). Representative image projections taken using confocal microscopy showed NP cells stained with

actin filament staining outside of both vehicle MPs (Fig. 5a) and BuOE MPs (Fig. 5b). Cross-sectional view of NP cells confirmed uptake vehicle MPs ranging between 4.03–12.81  $\mu\text{m}$  and BuOE MPs ranging between 2.04 and 23.89  $\mu\text{m}$  (Fig. 5c). Average diameter of BuOE MPs were internalized by NP cells ( $9.54 \pm 5.78 \mu\text{m}$ ) were significantly higher than diameter of internalized vehicle MPs ( $7.32 \pm 2.41 \mu\text{m}$ ) which is consistent with data above that BuOE MPs have significantly larger diameter than vehicle MPs. For context, the average NP cell diameter is  $15.4 \pm 5.1 \mu\text{m}$ . No visual differences or preferential uptake of BuOE MPs compared to vehicle MPs were observed through qualitative analysis. These results show that vehicle MPs and BuOE MPs do not adversely affect NP cells and MPs can be modified for intracellular or extracellular targeting by varying the size of MPs. Preliminary work has shown that increasing the homogenization speed significantly decreases vehicle MP diameter (Supplementary Fig. 3); however, these parameters have not been tested for BuOE MP fabrication.

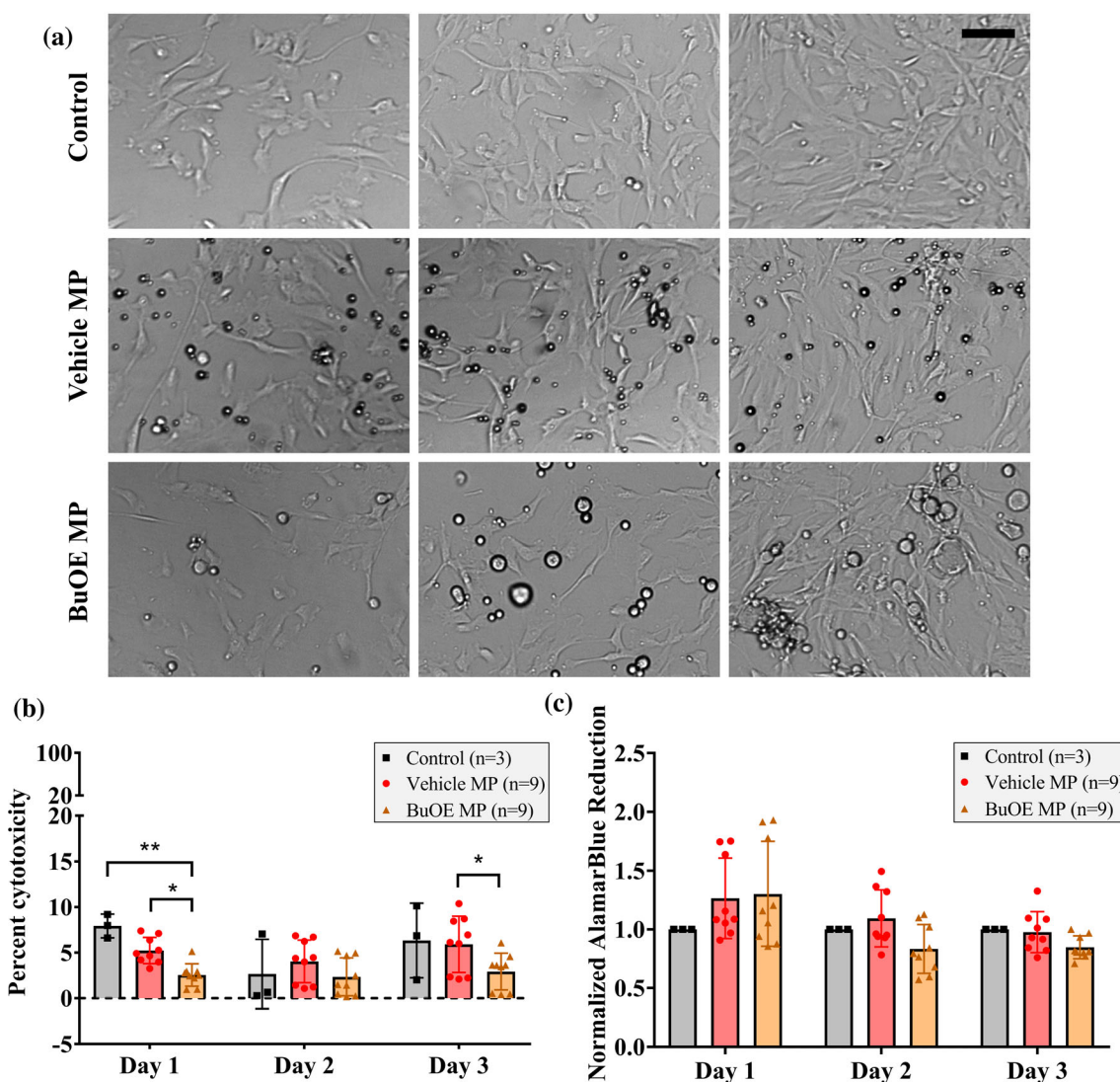


**FIGURE 4.** Vehicle MACS-A MPs and BuOE MPs are both cytocompatible with human nucleus pulposus (NP) cells in vitro. (a) Representative brightfield images of NP cell culture in vitro with and without MPs. Cells were able to proliferate and reach confluency comparable to control group after 3 days in culture with either vehicle MPs or BuOE MPs. Scale bar: 100  $\mu\text{m}$ . (b) LDH cytotoxicity assay measured less than 10% cytotoxicity levels in controls, vehicle MPs and BuOE MPs suggesting MPs are not cytotoxic to NP cells. No significant differences were detected in percent cytotoxicity of vehicle MPs compared to controls, while percent cytotoxicity of BuOE MPs were significantly lower than controls on day 1 and vehicle MPs on days 1 and 3. (c) Calculated cell metabolic activity using AlamarBlue assay was normalized to same-day control group. There were no significant differences in cell metabolic activity on days 1, 2 and 3 post-MP treatment which suggests MPs do not impact NP cellular metabolism. Bars and error bars represent mean and standard deviation between three control replicates and nine MP replicates (Three batches of MPs tested on three NP cell donors). \* $p < 0.05$ .

## DISCUSSION

Our results demonstrate that BuOE can be successfully encapsulated inside a MACS-A MP delivery vehicle with an average particle size of 22  $\mu\text{m}$ . The means of BuOE binding on the MACS-A MP matrix was not explored in this study. However, since manganese porphyrins are highly cationic<sup>6,65</sup> and CS are highly negatively charged polysaccharides that have the ability to bind positively charged molecules, BuOE could be loaded in the MPs *via* electrostatic interac-

tions.<sup>4,45</sup> The encapsulated BuOE slowly released over an 84-day time course where the non-released and released BuOE both maintains superoxide scavenging capacity. Further, this work is the first study to examine the effects of BuOE treatment and NP cells and demonstrate that vehicle and BuOE MPs are cytocompatible and can be internalized by NP cells.

ROS imbalance and oxidative stress are involved in the pathology of many age-related illnesses such as degenerative disc disease and osteoarthritis.<sup>33</sup> However, most treatments only treat the disease symptoms



such as pain and do not target the underlying causes of degeneration. Antioxidant therapeutics that scavenge ROS and restore oxidative balance can potentially be combined with current medications to be an effective treatment to halt disease progression. Previous studies have tested the antioxidative and protective effect of genistein<sup>80</sup> and catalase-loaded polymer capsules<sup>50</sup> from oxidative stress on NP cells. Targeting ROS with antioxidants can also reduce pain due to intervertebral disc degeneration as previous research has determined that ROS directly stimulates NP cells to secrete substance P, a neuropeptide transmitter involved in pain signaling.<sup>87</sup> In this work, we chose BuOE, a manganese porphyrin analog and SOD mimic, as a potential antioxidant therapeutic for applications in degenerative disc disease and osteoarthritis.

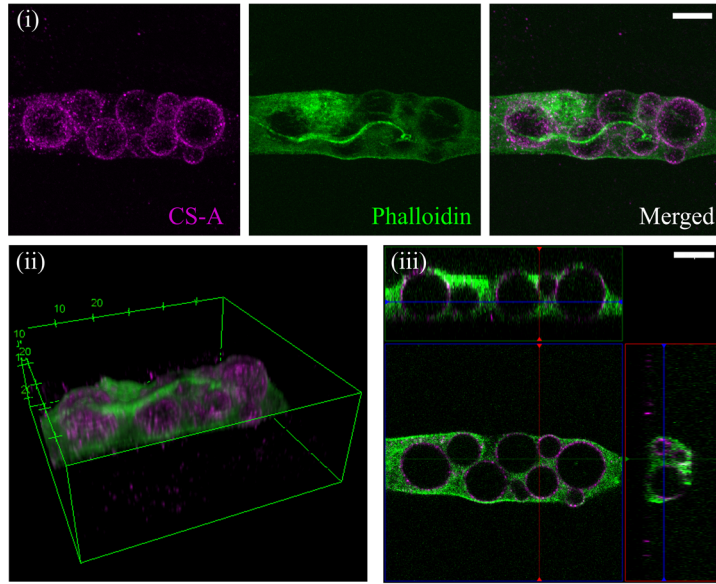
Manganese porphyrins have been researched for many decades and chemists have optimized the design of the redox-active compound to mimic SOD enzymes *in vivo*.<sup>5</sup> In comparison to other manganese porphyrins, BuOE was designed to be more lipophilic which allowed the drug to cross the blood brain barrier<sup>52</sup> and reduced cytotoxicity.<sup>65</sup> A limitation of BuOE pharmacokinetics is the rapid clearance from plasma and circulation after subcutaneous injection in mice.<sup>3</sup> One strategy to increase drug availability is to use micro/nanoparticles as delivery vehicles. To date, there are only few studies that have developed drug delivery systems as carriers for manganese porphyrins.<sup>1,41</sup> Schlichte *et al.* have shown encapsulating BuOE inside a lipid-coated silica nanoparticle resulted in slow release over 72 h *in vitro* which prevented hypotensive effects of BuOE after intraperitoneal injection *in vivo*.<sup>71</sup> Hence, particulate delivery systems with controlled drug release are needed to prevent adverse effects of naked BuOE. In this study, we have successfully encapsulated BuOE into chondroitin sulfate MPs as a drug delivery system and showed its cytocompatibility with NP cells. Nevertheless, *in vivo* assessments are needed to assess safety and dosing of our BuOE MP formulation.

Advancements in drug delivery research have engineered MPs as drug depots where the carrier can be tuned to slowly degrade and release the cargo,<sup>27</sup> thereby increasing drug retention in the local tissue. Our results demonstrate slow release of BuOE into the supernatant during 84-day incubation at 37 °C but did not observe any visible degradation of our vehicle and BuOE MPs after months of storage at either 37 °C, 4 °C, and – 20 °C. Preliminary testing to digest vehicle MPs showed they are robust and do not breakdown in the presence of chondroitinase or papain (data not shown). Therefore, BuOE released over months *in vitro* is likely due to passive diffusion. Our data also demonstrated that encapsulation of BuOE in MACS-

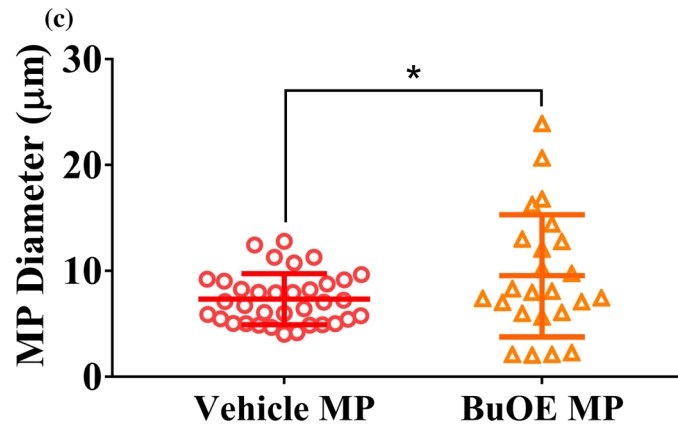
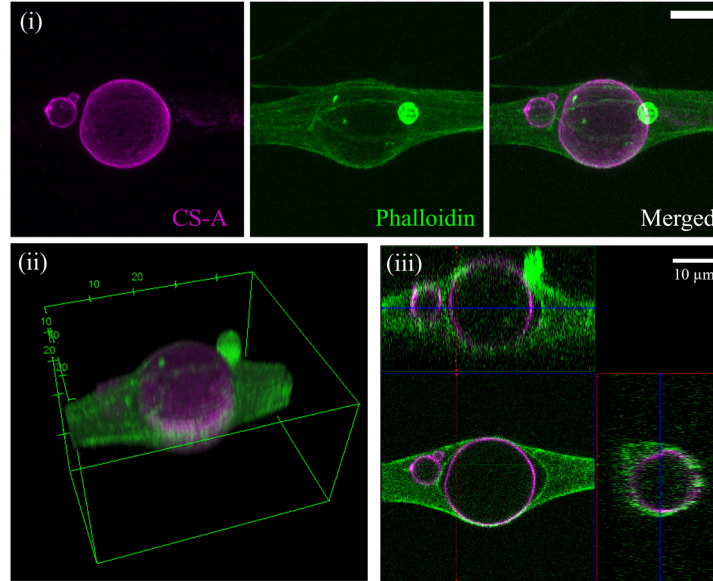
A MPs does not inhibit its superoxide scavenging ability but rather maintained its activity for up to 84 days after 37 °C incubation. The extended longevity of BuOE MPs superoxide scavenging activity compared to naked BuOE could be due to the combinatory effect of MACS-A since CS also has potential to scavenge ROS.<sup>15</sup> The self-renewing capabilities of BuOE also depends on the oxidation–reduction state of Mn<sup>3+</sup> as it can act as a pro-oxidant then cycling back to an Mn<sup>2+</sup> antioxidative state,<sup>5</sup> but more work is needed to understand BuOE recycling and how this phenomenon may change due to BuOE encapsulation. On the other hand, the decrease in superoxide scavenging activity of naked BuOE is consistent with previous anecdotal evidence that the drug itself loses its scavenging activity over time. However, it is unclear why the superoxide scavenging activity of naked BuOE dropped below zero on day 84. This may be a result of variability in xanthine oxidase enzyme activity between samples. The naked BuOE samples and assay blanks both received XO as a superoxide generator, but naked BuOE samples could have higher levels of superoxide generated than the negative controls blanks; hence, resulting in a negative percentage of superoxide scavenged for day 84 samples. Further research is needed to assess BuOE's lifespan and how the interaction between BuOE and MACS-A could positively increase or maintain superoxide scavenging ability. In addition, MPs have larger loading capacity compared to nanoparticles<sup>47</sup> and can be modified to increase loading volumes to further extend the availability of BuOE although release kinetics will need to be verified. Injecting BuOE MPs locally into degenerated discs or osteoarthritic cartilage may be a potential approach for long term ROS scavenging.

Further, these BuOE MPs are composed of predominantly CS-A. MACS-A MPs were selected as the vehicle for BuOE MPs because of the role of CS-A in maintaining healthy joints. Anti-catabolic properties of CS-A promoted its use as a supplement for treatment of osteoarthritis to strengthen and rebuild the articular cartilage ECM.<sup>34</sup> CS-A has also shown anti-inflammatory effects in osteoarthritis including reduction of joint swelling and preventing joint space narrowing.<sup>14,76</sup> CS-A can reduce pro-inflammatory cytokines such as TNF- $\alpha$  and IL-1 $\beta$  as well as ROS and reduce activation of MMPs.<sup>40</sup> CS-A also prevents IL-1 $\beta$ -induced p38MAPK phosphorylation and NF- $\kappa$ B nuclear translocation,<sup>40</sup> but the exact mechanism of how CS interact with cells to elicit this anti-inflammatory activity is not fully understood. CS-A also exhibits antioxidative properties *in vitro* which may help contribute to its anti-inflammatory effects.<sup>15,20,77</sup> Our DMMB staining of CS clearly demonstrates that our vehicle and BuOE MPs have robust amounts of CS

**(a) Vehicle MP**



**(b) BuOE MP**



◀ **FIGURE 5. NP cells uptake vehicle and BuOE MPs.** Human NP cells cultured with 100  $\mu\text{g}/\text{mL}$  (a) vehicle MPs or (b) BuOE MPs were fixed and labelled with actin using Phalloidin (green) while MPs were stained with CS-A antibody (magenta). (i) Maximum intensity projection of Z-stack fluorescent images show vehicle and BuOE MPs colocalized with NP cells. (ii) 3D view revealed NP cells surrounding and closely attaching onto MPs. (iii) 2D cross-sectional views confirmed that MPs were internalized by the NP cells as seen with positive actin staining enveloping the MPs. A single NP cell can also uptake more than one MP. (c) Internalized BuOE MPs were significantly larger in diameter compared to internalized vehicle MPs. Average diameter of vehicle MPs taken up by NP cells was  $7.32 \pm 2.41 \mu\text{m}$  while for internalized BuOE MPs, average diameter was  $9.54 \pm 5.78 \mu\text{m}$ . Error bars represent the average and standard deviation of vehicle MP (35 MPs) and BuOE MP (24 MPs) diameter internalized by NP cells. Scale bar: 10  $\mu\text{m}$ , \* $p < 0.05$ .

present and thus the use of MACS-A MPs for delivering BuOE credits further investigation for potential additional benefits such as reducing inflammation and healing joint tissues.

Interestingly, the LDH assay revealed that BuOE MPs significantly decreased apoptosis of NP cells compared to control cells. These data suggest that BuOE may have some anti-apoptotic effect. Previous literature has consistently shown BuOE and other manganese porphyrins enhance apoptosis in cancer cells while preserving healthy cells.<sup>43,85</sup> This differential effect on normal versus cancer cells could be due to the altered redox environment in cancer. Further study is needed into the NP cell redox environment and mechanisms of BuOE anti-apoptotic effect to understand these effects.

Our *in vitro* data also demonstrated that MPs were clearly taken up by NP cells. Superoxide is mainly generated in the mitochondria and released into the cytosol during cell respiration and cannot cross the cell membrane, thus release of BuOE from MPs and NP cells internalization of the BuOE MPs is essential to function. While naked BuOE readily crosses the cell membrane,<sup>53</sup> cellular uptake of BuOE MPs provides additional access to scavenging capacity for long term intracellular ROS scavenging. MP uptake could further enhance retention of BuOE at the site of administration. Thus, our findings of robust uptake of BuOE MPs could help facilitate decreasing intracellular superoxide. Additionally, MACS-A MP fabrication can be modified to form smaller MPs to facilitate intracellular ROS scavenging as noted in Supplemental Fig. 3. The size of internalized MPs is large, ranging up to 22  $\mu\text{m}$ . Nevertheless, this result is not surprising since NP cells are phagocytic in nature.<sup>44</sup> Jones *et al.* demonstrated NP cells ingesting latex beads as efficiently as phagocytic cells such as monocytes, macrophages and apoptotic cells.<sup>44</sup> A

potential route of internalization could be *via* the hyaluronan receptor for endocytosis (HARE), a scavenger receptor for hyaluronan, chondroitin sulfate and dermatan sulfate.<sup>31</sup> Chondrocytes express HARE to internalize hyaluronan,<sup>36</sup> but it is unclear whether NP cells which are chondrocyte-like cells also express HARE to bind and internalize CS.

A major limitation of this work is the lack of exploration of the ability of BuOE MPs to prevent or alleviate oxidative damage in NP cells. However, extensive literature has demonstrated that BuOE and other manganese porphyrins can prevent oxidative damage in fibroblasts,<sup>48</sup> neurons,<sup>37</sup> and chondrocytes<sup>16,19</sup> by scavenging ROS and simultaneously reducing senescence and inflammation. Thus, we believe that BuOE MPs will be able to have similar healing effects in degenerate NP cells. Future work will include validation that BuOE MPs can prevent or alleviate oxidative damage in NP cells. Downstream byproducts and signaling pathways after BuOE MP treatment can also be characterized to determine the mechanism of reduction in oxidative damage. In conclusion, we have demonstrated that BuOE MPs can be successfully fabricated and maintain potent superoxide scavenging capabilities up to 84-days. Furthermore, BuOE MPs are not cytotoxic and can be taken up by NP cells and thus hold the potential for reducing oxidative damage in disease states.

## SUPPLEMENTARY INFORMATION

The online version contains supplementary material available at <https://doi.org/10.1007/s12195-022-00744-w>.

## ACKNOWLEDGMENTS

This research was funded in part by the Nebraska Collaboration Initiative and the Nebraska Tobacco Settlement Biomedical Research Development Fund. The research was performed in part in the Nebraska Nanoscale Facility: National Nanotechnology Coordinated Infrastructure and the Nebraska Center for Materials and Nanoscience (and/or NERCF), which are supported by the National Science Foundation under Award ECCS: 1542182, and the Nebraska Research Initiative. We would like to thank Dr. Javier Seravalli at the University of Nebraska Lincoln Spectroscopy core facility for consultation on analysis and conducting the ICP-MS.



## CONFLICT OF INTEREST

Dr. Oberley-Deegan is a consultant with BioMimetix Pharmaceutical, Inc. and hold equities in BioMimetix Pharmaceutical, Inc.. All other authors have no conflicts of interest to disclose.

## DISCLAIMER

None.

## REFERENCES

- <sup>1</sup>Aikawa, T., S. Ito, M. Shinohara, M. Kaneko, T. Kondo, and M. Yuasa. A drug formulation using an alginate hydrogel matrix for efficient oral delivery of the manganese porphyrin-based superoxide dismutase mimic. *Biomater. Sci.* 3(6):861–869, 2015.
- <sup>2</sup>Anselmo, W., E. Branchetti, J. B. Grau, G. Li, S. Ayoub, E. K. Lai, et al. Porphyrin-based SOD mimic MnTnBu OE-2-PyP5+ inhibits mechanisms of aortic valve remodeling in human and murine models of aortic valve sclerosis. *J. Am. Heart Assoc.* 7(20):e007861, 2018.
- <sup>3</sup>Ashcraft, K. A., M.-K. Boss, A. Tovmasyan, K. R. Choudhury, A. N. Fontanella, K. H. Young, et al. Novel manganese-porphyrin superoxide dismutase-mimetic widens the therapeutic margin in a preclinical head and neck cancer model. *Int. J. Radiat. Oncol. Biol. Phys.* 93(4):892–900, 2015.
- <sup>4</sup>Bali J.-P., H. Cousse, E. Neuzil, editors. Biochemical basis of the pharmacologic action of chondroitin sulfates on the osteoarticular system. *Semin. Arthritis Rheum.* 2001.
- <sup>5</sup>Batinic-Haberle, I., A. Tovmasyan, and I. Spasojevic. An educational overview of the chemistry, biochemistry and therapeutic aspects of Mn porphyrins—from superoxide dismutation to H<sub>2</sub>O<sub>2</sub>-driven pathways. *Redox Biol.* 5:43–65, 2015.
- <sup>6</sup>Batinic-Haberle, I., A. Tovmasyan, and I. Spasojevic. Mn porphyrin-based redox-active therapeutics. *Redox-active therapeutics*. New York: Springer, pp. 165–212, 2016.
- <sup>7</sup>Batinic-Haberle, I., A. Tovmasyan, and I. Spasojevic. Mn porphyrin-based redox-active drugs: differential effects as cancer therapeutics and protectors of normal tissue against oxidative injury. *Antioxid. Redox Signal.* 29(16):1691–1724, 2018.
- <sup>8</sup>Birben, E., U. M. Sahiner, C. Sackesen, S. Erzurum, and O. Kalayci. Oxidative stress and antioxidant defense. *World Allergy Org. J.* 5(1):9–19, 2012.
- <sup>9</sup>Bjarnason, I., and J. Hayllar. Side effects of nonsteroidal anti-inflammatory drugs on the small and large intestine in humans. *Gastroenterology.* 104(6):1832–1847, 1993.
- <sup>10</sup>Bobinac, D., J. Spanjol, S. Zoricic, and I. Maric. Changes in articular cartilage and subchondral bone histomorphometry in osteoarthritic knee joints in humans. *Bone.* 32(3):284–290, 2003.
- <sup>11</sup>Bolduc, J. A., J. A. Collins, and R. F. Loeser. Reactive oxygen species, aging and articular cartilage homeostasis. *Free Radic. Biol. Med.* 132:73–82, 2019.
- <sup>12</sup>Brantigan, J. W., A. Neidre, and J. S. Toohey. The lumbar I/F cage for posterior lumbar interbody fusion with the variable screw placement system: 10-year results of a Food and Drug Administration clinical trial. *Spine J.* 4(6):681–688, 2004.
- <sup>13</sup>Butoescu, N., O. Jordan, and E. Doelker. Intra-articular drug delivery systems for the treatment of rheumatic diseases: a review of the factors influencing their performance. *Eur. J. Pharm. Biopharm.* 73(2):205–218, 2009.
- <sup>14</sup>Campo, G. M., A. Avenoso, S. Campo, A. M. Ferlazzo, D. Altavilla, and A. Calatroni. Efficacy of treatment with glycosaminoglycans on experimental collagen-induced arthritis in rats. *Arthritis Res Ther.* 5(3):1–10, 2003.
- <sup>15</sup>Campo, G., A. Avenoso, S. Campo, A. Ferlazzo, and A. Calatroni. Antioxidant activity of chondroitin sulfate. *Adv. Pharmacol.* 53:417–431, 2006.
- <sup>16</sup>Campo, G. M., A. Avenoso, A. D’Ascola, M. Scuruchi, G. Nastasi, A. Micali, et al. The SOD mimic MnTM-2-PyP (5+) reduces hyaluronan degradation-induced inflammation in mouse articular chondrocytes stimulated with Fe (II) plus ascorbate. *Int. J. Biochem. Cell Biol.* 45(8):1610–1619, 2013.
- <sup>17</sup>Chandel, N. S., W. C. Trzyna, D. S. McClintock, and P. T. Schumacker. Role of oxidants in NF- $\kappa$ B activation and TNF- $\alpha$  gene transcription induced by hypoxia and endotoxin. *J. Immunol.* 165(2):1013–1021, 2000.
- <sup>18</sup>Chatterjee, A., Y. Zhu, Q. Tong, E. A. Kosmacek, E. Z. Lichter, and R. E. Oberley-Deegan. The addition of manganese porphyrins during radiation inhibits prostate cancer growth and simultaneously protects normal prostate tissue from radiation damage. *Antioxidants.* 7(1):21, 2018.
- <sup>19</sup>Coleman, M. C., M. J. Brouillette, N. S. Andresen, R. E. Oberley-Deegan, and J. M. Martin. Differential effects of superoxide dismutase mimetics after mechanical overload of articular cartilage. *Antioxidants.* 6(4):98, 2017.
- <sup>20</sup>Craciunescu, O., L. Moldovan, M. Moisei, and M. Trif. Liposomal formulation of chondroitin sulfate enhances its antioxidant and anti-inflammatory potential in L929 fibroblast cell line. *J. Liposome Res.* 23(2):145–153, 2013.
- <sup>21</sup>Cross, M., E. Smith, D. Hoy, S. Nolte, I. Ackerman, M. Fransen, et al. The global burden of hip and knee osteoarthritis: estimates from the global burden of disease 2010 study. *Ann. Rheum. Dis.* 73(7):1323–1330, 2014.
- <sup>22</sup>DePalma, M. J., J. M. Ketchum, and T. Saullo. What is the source of chronic low back pain and does age play a role? *Pain Med.* 12(2):224–233, 2011.
- <sup>23</sup>Dimozi, A., E. Mavrogonatou, A. Sklirou, and D. Kletsas. Oxidative stress inhibits the proliferation, induces premature senescence and promotes a catabolic phenotype in human nucleus pulposus intervertebral disc cells. *Eur. Cells Mater.* 30:89–103, 2015. <https://doi.org/10.22203/eCM.v030a07>.
- <sup>24</sup>Evans, C. H., S. C. Ghivizzani, and P. D. Robbins. Gene delivery to joints by intra-articular injection. *Hum. Gene Therapy.* 29(1):2–14, 2018.
- <sup>25</sup>Faulkner, K. M., S. I. Liochev, and I. Fridovich. Stable Mn (III) porphyrins mimic superoxide dismutase in vitro and substitute for it in vivo. *J. Biol. Chem.* 269(38):23471–23476, 1994.
- <sup>26</sup>Feng, C., M. Yang, M. Lan, C. Liu, Y. Zhang, B. Huang, et al. ROS: crucial intermediators in the pathogenesis of intervertebral disc degeneration. *Oxidat. Med. Cell. Longev.* 2017.
- <sup>27</sup>Fenton, O. S., K. N. Olafson, P. S. Pillai, M. J. Mitchell, and R. Langer. Advances in biomaterials for drug delivery. *Adv. Mater.* 30(29):1705328, 2018.
- <sup>28</sup>Gad, S. C., D. W. Sullivan Jr., I. Spasojevic, C. V. Mujer, C. B. Spainhour, and J. D. Crapo. Nonclinical safety and

- toxicokinetics of MnTnBuOE-2-PyP5+ (BMX-001). *Int. J. Toxicol.* 35(4):438–453, 2016.
- <sup>29</sup>Goude, M. C., T. C. McDevitt, and J. S. Temenoff. Chondroitin sulfate microparticles modulate transforming growth factor- $\beta$ 1-induced chondrogenesis of human mesenchymal stem cell spheroids. *Cells Tissues Organs.* 199(2–3):117–130, 2014.
- <sup>30</sup>Han, Y., X. Li, M. Yan, M. Yang, S. Wang, J. Pan, et al. Oxidative damage induces apoptosis and promotes calcification in disc cartilage endplate cell through ROS/MAPK/NF- $\kappa$ B pathway: implications for disc degeneration. *Biochem. Biophys. Res. Commun.* 516(3):1026–1032, 2019.
- <sup>31</sup>Harris, E. N., and P. H. Weigel. The ligand-binding profile of HARE: hyaluronan and chondroitin sulfates A, C, and D bind to overlapping sites distinct from the sites for heparin, acetylated low-density lipoprotein, dermatan sulfate, and CS-E. *Glycobiology.* 18(8):638–648, 2008.
- <sup>32</sup>Healy, W. L., C. J. Della Valle, R. Iorio, K. R. Berend, F. D. Cushman, D. F. Dalury, et al. Complications of total knee arthroplasty: standardized list and definitions of the Knee Society. *Clin. Orthop. Relat. Res.* 471(1):215–220, 2013.
- <sup>33</sup>Henrotin, Y., P. Bruckner, and J.-P. Pujol. The role of reactive oxygen species in homeostasis and degradation of cartilage. *Osteoarthritis Cartil.* 11(10):747–755, 2003.
- <sup>34</sup>Henrotin, Y., M. Mathy, C. Sanchez, and C. Lambert. Chondroitin sulfate in the treatment of osteoarthritis: from in vitro studies to clinical recommendations. *Therap. Adv. Musculoskelet. Dis.* 2(6):335–348, 2010.
- <sup>35</sup>Hoy, D., C. Bain, G. Williams, L. March, P. Brooks, F. Blyth, et al. A systematic review of the global prevalence of low back pain. *Arthritis Rheum.* 64(6):2028–2037, 2012.
- <sup>36</sup>Hua, Q., C. B. Knudson, and W. Knudson. Internalization of hyaluronan by chondrocytes occurs via receptor-mediated endocytosis. *J. Cell Sci.* 106(1):365–375, 1993.
- <sup>37</sup>Huang, H. F., F. Guo, Y. Z. Cao, W. Shi, and Q. Xia. Neuroprotection by manganese superoxide dismutase (Mn SOD) mimics: antioxidant effect and oxidative stress regulation in acute experimental stroke. *CNS Neurosci. Therap.* 18(10):811–818, 2012.
- <sup>38</sup>Hybertson, B. M., B. Gao, S. K. Bose, and J. M. McCord. Oxidative stress in health and disease: the therapeutic potential of Nrf2 activation. *Mol. Aspects Med.* 32(4–6):234–246, 2011.
- <sup>39</sup>Ighodaro, O., and O. Akinloye. First line defence antioxidants-superoxide dismutase (SOD), catalase (CAT) and glutathione peroxidase (GPX): their fundamental role in the entire antioxidant defence grid. *Alex. J. Med.* 54(4):287–293, 2018.
- <sup>40</sup>Iovu, M., G. Dumais, and P. Du Souich. Anti-inflammatory activity of chondroitin sulfate. *Osteoarthritis Cartil.* 16:S14–S18, 2008.
- <sup>41</sup>Ito, F., H. Yamada, K. Kanamura, and H. Kawakami. Preparation of biodegradable polymer nanospheres containing manganese porphyrin (Mn-porphyrin). *J. Inorg. Organomet. Polym. Mater.* 29(3):1010–1018, 2019.
- <sup>42</sup>Janssen, M., G. Mihov, T. Welting, J. Thies, and P. Emans. Drugs and polymers for delivery systems in OA joints: clinical needs and opportunities. *Polymers.* 6(3):799–819, 2014.
- <sup>43</sup>Jaramillo, M. C., M. M. Briehl, J. D. Crapo, I. Batinic-Haberle, and M. E. Tome. Manganese porphyrin, MnTE-2-PyP5+, acts as a pro-oxidant to potentiate glucocorticoid-induced apoptosis in lymphoma cells. *Free Radic. Biol. Med.* 52(8):1272–1284, 2012.
- <sup>44</sup>Jones, P., L. Gardner, J. Menage, G. T. Williams, and S. Roberts. Intervertebral disc cells as competent phagocytes in vitro: implications for cell death in disc degeneration. *Arthritis Res. Therapy.* 10(4):1–8, 2008.
- <sup>45</sup>Kim, H. D., E. A. Lee, Y.-H. An, S. L. Kim, S. S. Lee, S. J. Yu, et al. Chondroitin sulfate-based biomimetic surface hydrogels for bone tissue engineering. *ACS Appl. Mater. Interfaces.* 9(26):21639–21650, 2017.
- <sup>46</sup>Kim, J., M. Xu, R. Xo, A. Mates, G. Wilson, A. Pearsall IV., et al. Mitochondrial DNA damage is involved in apoptosis caused by pro-inflammatory cytokines in human OA chondrocytes. *Osteoarthritis Cartil.* 18(3):424–432, 2010.
- <sup>47</sup>Kohane, D. S. Microparticles and nanoparticles for drug delivery. *Biotechnol. Bioeng.* 96(2):203–209, 2007. <https://doi.org/10.1002/bit.21301>.
- <sup>48</sup>Kosmacek, E. A., A. Chatterjee, Q. Tong, C. Lin, and R. E. Oberley. MnTnBuOE-2-PyP protects normal colorectal fibroblasts from radiation damage and simultaneously enhances radio/chemotherapeutic killing of colorectal cancer cells. *Oncotarget.* 7(23):34532, 2016.
- <sup>49</sup>Laine, L., S. Curtis, B. Cryer, A. Kaur, and C. Cannon. Risk factors for NSAID-associated upper GI clinical events in a long-term prospective study of 34 701 arthritis patients. *Aliment. Pharmacol. Therap.* 32(10):1240–1248, 2010.
- <sup>50</sup>Larrañaga, A., I. L. M. Isa, V. Patil, S. Thamboo, M. Lomora, M. A. Fernández-Yague, et al. Antioxidant functionalized polymer capsules to prevent oxidative stress. *Acta Biomater.* 67:21–31, 2018.
- <sup>51</sup>Lengyel, M., N. Kállai-Szabó, V. Antal, A. J. Laki, and I. Antal. Microparticles, microspheres, and microcapsules for advanced drug delivery. *Sci. Pharm.* 87(3):20, 2019.
- <sup>52</sup>Leu, D., I. Spasojevic, H. Nguyen, B. Deng, A. Tovmasyan, T. Weitner, et al. CNS bioavailability and radiation protection of normal hippocampal neurogenesis by a lipophilic Mn porphyrin-based superoxide dismutase mimic, MnTnBuOE-2-PyP5+. *Redox Biol.* 12:864–871, 2017.
- <sup>53</sup>Li, A. M., J. Martins, A. Tovmasyan, J. S. Valentine, I. Batinic-Haberle, I. Spasojevic, et al. Differential localization and potency of manganese porphyrin superoxide dismutase-mimicking compounds in *Saccharomyces cerevisiae*. *Redox Biol.* 3:1–6, 2014.
- <sup>54</sup>Lim, J. J., T. M. Hammoudi, A. M. Bratt-Leal, S. K. Hamilton, K. L. Kepple, N. C. Bloodworth, et al. Development of nano- and microscale chondroitin sulfate particles for controlled growth factor delivery. *Acta Biomater.* 2011. <https://doi.org/10.1016/j.actbio.2010.10.009>.
- <sup>55</sup>Mapuskar K. A., C.M. Anderson, D.R. Spitz, I. Batinic-Haberle, B.G. Allen, R.E. Oberley-Deegan, editors. Utilizing superoxide dismutase mimetics to enhance radiation therapy response while protecting normal tissues. *Semin. Radiat. Oncol.* (2019).
- <sup>56</sup>Marin, E., C. Tapeinos, S. Lauciello, G. Ciofani, J. Sarasua, and A. Larrañaga. Encapsulation of manganese dioxide nanoparticles into layer-by-layer polymer capsules for the fabrication of antioxidant microreactors. *Mater. Sci. Eng. C.* 117:111349, 2020.
- <sup>57</sup>Mittal, M., M. R. Siddiqui, K. Tran, S. P. Reddy, and A. B. Malik. Reactive oxygen species in inflammation and tissue injury. *Antioxid. Redox Signal.* 20(7):1126–1167, 2014.
- <sup>58</sup>Mittler, R. ROS are good. *Trends Plant Sci.* 22(1):11–19, 2017.

- <sup>59</sup>Naik, E., and V. M. Dixit. Mitochondrial reactive oxygen species drive proinflammatory cytokine production. *J. Exp. Med.* 208(3):417–420, 2011.
- <sup>60</sup>Nakaoka, R., Y. Tabata, T. Yamaoka, and Y. Ikada. Prolongation of the serum half-life period of superoxide dismutase by poly (ethylene glycol) modification. *J. Control. Release.* 46(3):253–261, 1997.
- <sup>61</sup>Nasto, L. A., A. R. Robinson, K. Ngo, C. L. Clauson, Q. Dong, C. St. Croix, et al. Mitochondrial-derived reactive oxygen species (ROS) play a causal role in aging-related intervertebral disc degeneration. *J. Orthop. Res.* 31(7):1150–1157, 2013.
- <sup>62</sup>Nettles, D. L., T. P. Vail, M. T. Morgan, M. W. Grinstaff, and L. A. Setton. Photocrosslinkable hyaluronan as a scaffold for articular cartilage repair. *Ann. Biomed. Eng.* 32(3):391–397, 2004.
- <sup>63</sup>Otsuki, S., M. Nakajima, M. Lotz, and M. Kinoshita. Hyaluronic acid and chondroitin sulfate content of osteoarthritic human knee cartilage: site-specific correlation with weight-bearing force based on femorotibial angle measurement. *J. Orthop. Res.* 26(9):1194–1198, 2008.
- <sup>64</sup>Page, J., and D. Henry. Consumption of NSAIDs and the development of congestive heart failure in elderly patients: an underrecognized public health problem. *Arch. Intern. Med.* 160(6):777–784, 2000.
- <sup>65</sup>Rajic, Z., A. Tovmasyan, I. Spasojevic, H. Sheng, M. Lu, A. M. Li, et al. A new SOD mimic, Mn (III) ortho N-butoxyethylpyridylporphyrin, combines superb potency and lipophilicity with low toxicity. *Free Radic. Biol. Med.* 52(9):1828–1834, 2012.
- <sup>66</sup>Ratcliffe, J., I. Hunneyball, C. Wilson, A. Smith, and S. Davis. Albumin microspheres for intra-articular drug delivery: investigation of their retention in normal and arthritic knee joints of rabbits. *J. Pharmacy Pharmacol.* 39(4):290–295, 1987.
- <sup>67</sup>Ray, P. D., B.-W. Huang, and Y. Tsuji. Reactive oxygen species (ROS) homeostasis and redox regulation in cellular signaling. *Cell. Signal.* 24(5):981–990, 2012.
- <sup>68</sup>Romereim, S. M., C. A. Johnston, A. L. Redwine, and R. A. Wachs. Development of an in vitro intervertebral disc innervation model to screen neuroinhibitory biomaterials. *J. Orthop. Res.* 38(5):1016–1026, 2020.
- <sup>69</sup>Schlichte, S. L., S.-Y. Park, E. A. Kosmacek, K. Katsurada, K. P. Patel, R. E. Oberley-Deegan, et al. Clinically-tested SOD mimic, MnTnBuOE-2-PyP5+, acutely decreases blood pressure via sympathoinhibition and vasodilation. *FASEB J.* 34(S1):1, 2020.
- <sup>70</sup>Schlichte, S. L., E. J. Pekas, T. J. Bruett, E. A. Kosmacek, B. T. Hackfort, J. M. Rasmussen, et al. Sympathoinhibition and vasodilation contribute to the acute hypotensive response of the superoxide dismutase mimic, MnTnBuOE-2-PyP5+, in hypertensive animals. *Adv. Redox Res.* 3:100016, 2021.
- <sup>71</sup>Schlichte S. L., S. Romanova, K. Katsurada, E.A. Kosmacek, T.K. Bronich, K.P. Patel, et al. Nanoformulation of the superoxide dismutase mimic, MnTnBuOE-2-PyP5+, prevents its acute hypotensive response. *Redox Biol.* 2020:101610.
- <sup>72</sup>Singh, G., and G. Triadafilopoulos. Epidemiology of NSAID induced gastrointestinal complications. *J. Rheumatol. Suppl.* 56:18–24, 1999.
- <sup>73</sup>Sivan, S. S., A. J. Hayes, E. Wachtel, B. Caterson, Y. Merkher, A. Maroudas, et al. Biochemical composition and turnover of the extracellular matrix of the normal and degenerate intervertebral disc. *Eur. Spine J.* 23(3):344–353, 2014.
- <sup>74</sup>Smeds, K. A., and M. W. Grinstaff. Photocrosslinkable polysaccharides for in situ hydrogel formation. *J. Biomed. Mater. Res.* 54(1):115–121, 2001.
- <sup>75</sup>Tovmasyan, A., R. S. Sampaio, M.-K. Boss, J. C. Bueno-Janice, B. H. Bader, M. Thomas, et al. Anticancer therapeutic potential of Mn porphyrin/ascorbate system. *Free Radic. Biol. Med.* 89:1231–1247, 2015.
- <sup>76</sup>Uebelhart, D., M. Malaise, R. Marcolongo, F. DeVathaire, M. Piperno, E. Mailleux, et al. Intermittent treatment of knee osteoarthritis with oral chondroitin sulfate: a one-year, randomized, double-blind, multicenter study versus placebo. *Osteoarthr. Cartil.* 12(4):269–276, 2004.
- <sup>77</sup>Vallières, M., and P. Du Souich. Modulation of inflammation by chondroitin sulfate. *Osteoarthr. Cartil.* 18:S1–S6, 2010.
- <sup>78</sup>Vos, T., C. Allen, M. Arora, R. M. Barber, Z. A. Bhutta, A. Brown, et al. Global, regional, and national incidence, prevalence, and years lived with disability for 310 diseases and injuries, 1990–2015: a systematic analysis for the Global Burden of Disease Study 2015. *Lancet.* 388(10053):1545–1602, 2016.
- <sup>79</sup>Wang H., L. Ma, D. Yang, T. Wang, S. Liu, S. Yang, et al. Incidence and risk factors of adjacent segment disease following posterior decompression and instrumented fusion for degenerative lumbar disorders. *Medicine.* 2017;96(5).
- <sup>80</sup>Wang, K., S. Hu, B. Wang, J. Wang, X. Wang, and C. Xu. Genistein protects intervertebral discs from degeneration via Nrf2-mediated antioxidant defense system: an in vitro and in vivo study. *J. Cell. Physiol.* 234(9):16348–16356, 2019.
- <sup>81</sup>Wang, L.-F., S.-S. Shen, and S.-C. Lu. Synthesis and characterization of chondroitin sulfate-methacrylate hydrogels. *Carbohydr. Polym.* 52(4):389–396, 2003.
- <sup>82</sup>Whelton A., and A.J. Watson. Nonsteroidal anti-inflammatory drugs: effects on kidney function. *Clin. Nephrotox.* 1998:203–216.
- <sup>83</sup>Wickens, A. P. Ageing and the free radical theory. *Respir. Physiol.* 128(3):379–391, 2001.
- <sup>84</sup>Yang, J., M. Shen, H. Wen, Y. Luo, R. Huang, L. Rong, et al. Recent advance in delivery system and tissue engineering applications of chondroitin sulfate. *Carbohydr. Polym.* 230:115650, 2020.
- <sup>85</sup>Yulyana, Y., A. Tovmasyan, I. A. Ho, K. C. Sia, J. P. Newman, W. H. Ng, et al. Redox-active Mn porphyrin-based potent SOD mimic, MnTnBuOE-2-PyP5+, enhances carbenoxolone-mediated TRAIL-induced apoptosis in glioblastoma multiforme. *Stem Cell Rev. Rep.* 12(1):140–155, 2016.
- <sup>86</sup>Zhao, Y., D. W. Carroll, Y. You, L. Chaiswing, R. Wen, I. Batinic-Haberle, et al. A novel redox regulator, MnTnBuOE-2-PyP5+, enhances normal hematopoietic stem/progenitor cell function. *Redox Biol.* 12:129–138, 2017.
- <sup>87</sup>Zheng J., J. Zhang, X. Zhang, Z. Guo, W. Wu, Z. Chen, et al. Reactive oxygen species mediate low back pain by



upregulating substance p in intervertebral disc degeneration. *Oxidat. Med. Cell. Longev.* 2021;2021.

**Publisher's Note** Springer Nature remains neutral with regard to jurisdictional claims in published maps and institutional affiliations.

Springer Nature or its licensor holds exclusive rights to this article under a publishing agreement with the author(s) or other rightsholder(s); author self-archiving of the accepted manuscript version of this article is solely governed by the terms of such publishing agreement and applicable law.